Growth of Grains and Correlated Grain Clusters in a Block Copolymer Melt

M. C. Newstein, B. A. Garetz,* N. P. Balsara,* M. Y. Chang, and H. J. Dai

Departments of Electrical Engineering and Chemical Engineering, Chemistry & Materials Science, Polytechnic University, Six Metrotech Center, Brooklyn, New York 11201

Received July 18, 1997; Revised Manuscript Received October 27, 1997

ABSTRACT: Ordering kinetics after quenching a block copolymer melt from the disordered state to the ordered state were studied by time-resolved, depolarized light scattering. A theoretical framework for relating the scattering patterns to the granular organization within the sample was developed. In some cases we found that ordering proceeds by the growth of individual grains. These systems were characterized by scattering profiles that are monotonic functions of scattering angle. In contrast, the scattering profiles, under certain quench conditions, contained peaks indicating the presence of intergrain correlations. We demonstrate that these correlations arise due to the presence of three-dimensional grain clusters. Estimates of the size, shape, and concentration of grains during the transformation from disorder to order were obtained. In the early stages of ordering, the grains grew quickly at the expense of the disordered phase until the entire sample was occupied by grains. This stage was followed by extremely slow grain growth (or undetectable growth, in the case of large quench depths) due to defect annihilation.

Introduction

Block copolymers are known to form ordered phases composed of lamellae, cylinders, and spheres, as well as a diversity of other structures.[1] Similar phases are found in other materials such as surfactant solutions and assemblies of rodlike molecules.[2] The equilibrium behavior of these systems is reasonably well-understood, and a unified framework for predicting microstructure in these diverse systems has recently been proposed.[3] However, little is known about the kinetics of order formation in these materials.[3] Block copolymers are ideally suited for such studies because of easy access to the disordered phase, which is a convenient initial state for such studies. In addition, slow dynamics of polymer chains, due to phenomena such as entanglement and proximity to a glass transition, enables time-resolved measurements with relative ease.

Harkless et al. used small-angle X-ray scattering to study the kinetics of ordering in a polystyrene-*block*-polybutadiene/*n*-tetradecane solution.[4] In these experiments, the ordered phase consisted of polystyrene spheres arranged on a crystal-like, body centered cubic (BCC) lattice. Quenching this system from the disordered to the ordered state resulted in the development of primary and higher-order peaks corresponding to the symmetry of the BCC phase. Evidence for slow ordering kinetics is contained in this early work. In subsequent years, SAXS has been used to study the evolution of lamellar order.[5−8] In these systems, quenching from the disordered to the ordered state results only in a sharpening of the primary maximum. Higher-order peaks are not evident several hours after initiating the ordering process. In such cases, only qualitative conclusions regarding the ordering kinetics can be made. Time-resolved rheological measurements are often used to study order formation in block copolymers.[9,10] These experiments are difficult to interpret because the relationship between the rheology and structure of partially ordered block copolymers remains unresolved.

Theoretical studies of nucleation and growth of the ordered phase in a lamellar block copolymer were conducted by Fredrickson and Binder.[11] More recently, Qi and Wang studied the transformation from cylinders to disorder by spinodal decomposition.[12] They demonstrated that the kinetic pathways for such transformations can be complex. In particular, they found that the disordering of cylinders can occur via the formation of a metastable cubic phase. Goveas and Milner computed the velocity at which the ordered phase is consumed by the disordered phase during an order-to-disorder transition.[13] Computer simulations of ordering kinetics in block copolymer melts have also been conducted.[14]

This paper is part of a series on the relationship between optical properties and grain structure of quiescently ordered block copolymers.[15−19] Individual, ordered grains in lamellar and cylindrical block copolymers are equivalent to uniaxial crystals. For samples with a cylindrical morphology, the optic axis is parallel to the axes of the cylinders. The simplest situation arises if the sample is composed of individual, randomly shaped grains with (1) a constant optic axis within a grain, (2) no correlation between grain shape and optic axis, and (3) no correlation between optic axes of different grains. We refer to such a system as "ideal grains". In ref 15 we studied the propagation of polarized light through a collection of ideal grains and showed that the total intensity of light leaking through such a sample, held between crossed polarizers, is proportional to the average grain size. That analysis[15] was restricted to samples with grains that are much larger than the wavelength of light. In a subsequent paper, we studied depolarized scattering in these systems, which becomes increasingly important as the grain size becomes comparable to the wavelength of light.[16] We compared grain sizes measured by depolarized scattering with direct images obtained by transmission electron microscopy.[17] This analysis showed that one could maintain the concept of grain correlation length even in cases where the local optic axis exhibited significant continuous variation with position. At this point the relationship

* Authors to whom correspondence should be addressed.

S0024-9297(97)01086-3 CCC: $15.00
Published on Web 01/13/1998

between optical properties and structure for the case of ideal grains is, to a large extent, well-understood.

The depolarized light scattering profiles from ideal grains are azimuthally symmetric. However, in several experiments[18,19] we have observed depolarized scattering profiles that are azimuthally asymmetric. This indicates that the grain structure is "nonideal"; i.e., one or more of the three criteria necessary for grain ideality (see previous paragraph) is no longer satisfied. Evidence for the existence of nonideal grain structures was also obtained by Hashimoto and Sakamoto, who conducted transmission electron microscopy on a lamellar polystyrene-*block*-polyisoprene copolymer during the ordering process.[7]

In this paper, we develop a unified theoretical framework for analyzing depolarized light scattering from grain structures that are not ideal. For simplicity, we assume that the sample is composed of grains with constant optic axis within each grain. However, we admit the possibility of obtaining intragrain correlations between grain shape and optic axis. Such correlations involve the relaxation of ideal-grain criterion 2 and give rise to azimuthally asymmetric light scattering profiles. We also include the possibility of obtaining clusters of grains wherein the orientation of the optic axes of the individual grains are correlated. Such intergrain correlations involve a relaxation of criterion 3 and give rise to off-axis light scattering maxima. This unified framework is used to analyze scattering data from a polystyrene-*block*-polyisoprene melt which exhibited an order-to-disorder transition at 59 °C. We measured the time dependence of the depolarized scattering profiles after thermally quenching from the disordered state to the ordered state. The grain structure was found to be a sensitive function of quench depth. Ideal grains were found when the quench depth was large and the quench temperature was in the vicinity of the glass transition temperature of the polystyrene block. On the other hand, nonideal grain structures were found when the quench depth was small and the quench temperature was above the glass transition temperature of the polystyrene block. The evolution of grain structure in these different cases is discussed. Our use of the time evolution of depolarized light scattering profiles owes much to the pioneering work of Stein and co-workers, who have used such information to infer the kinetics of the growth of domains in nematic liquid crystals.[20,21]

Experimental Procedure

A polystyrene-*block*-polyisoprene copolymer was synthesized by anionic polymerization under high vacuum. The molecular weights of the polystyrene and polyisoprene blocks are 4 and 13 kg/mol, respectively, and we refer to this sample as SI(4-13). This sample exhibits a disordered phase at temperatures above 59 °C and a cylindrical phase at temperatures below 59 °C, as was shown in previous publications using synchrotron X-ray scattering and the local birefringence method.[22] Differential scanning calorimetry (DSC) measurements at 10 °C/min revealed a glass transition at 51 °C.

A schematic of the instrument used for measuring the depolarized light scattering profiles is shown in Figure 1. A melt of SI(4-13) was placed between two fused quartz disks with an anodized Al spacer with a thickness of 5 mm. This assembly was placed in a temperature-controlled heating block. The temperature at the outer edge of the spacer was monitored, and the relationship between the monitored temperature and the sample temperature was established in separate experiments where a thermocouple was placed at the center of the polymer sample. The ordering kinetics in SI(4-13) was studied at four temperatures: 50.0, 52.0, 53.7, and 55.5 °C. The light from a laser was directed through a horizontal Glan air-spaced polarizer and a quarter-wave plate (compensator) before impinging on the sample. The light emerging from the sample passed through a large area dichroic polarizer and was projected onto a paper screen. Either a 100 mW continuous wave (cw), frequency-doubled Nd:YAG laser with $\lambda = 0.532\ \mu$m (Coherent DPS 532) or a 15 mW HeNe laser with $\lambda = 0.633\ \mu$m (Meles Griot) was used as the light source. Each quench was repeated several times and on different SI-(4−13) samples to ensure reproducibility. For the sake of clarity, we show one set of data at each temperature. Most of the data presented in this paper (except data at 52.0 °C for $t > 300$ min) were obtained using the Nd:YAG laser.

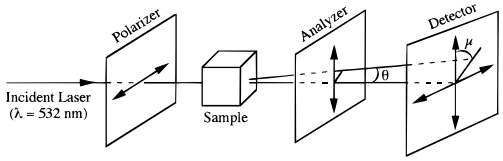

Figure 1. Schematic of depolarized light scattering instrument.

An MTI Dage CCD 72 camera equipped with a two-dimensional charge coupled device (CCD) with 8 bit resolution was used to capture the scattering profile projected onto the screen. The signal at selected pixels on the CCD was digitized by a Perceptics PixelPipeline digitizer, and the data were acquired by a Power Macintosh using LabVIEW. Before each experiment, the beam center was located by uncrossing the polarizer slightly and locating the pixel with the highest intensity. Data were recorded along two directions, $\mu = 0$ and $\mu = \pi/4$. The row of pixels corresponding to these directions was identified by a straightforward calibration procedure. The intensity along this row and two adjacent rows on either side were recorded with an exposure time of about 60 s, and the average of the five rows was taken as the scattering intensity along a given direction. In the $\mu = \pi/4$ case, we obtained four sets of scattering profiles along $\mu = \pm\pi/4$ and $\mu = \pm 3\pi/4$ which were averaged to obtain the final scattering profiles. In the $\mu = 0$ case only the vertical direction ($\mu = 0$ and π) was used. The magnitude of the scattering vector, $\mathbf{q}$, is defined by $q = 4\pi \sin(\theta/2)/\lambda$. The screen was mounted on a rail, and the sample-to-screen distance was increased from its initial value of 15 cm, to enlarge the scattering profile in cases where the pattern was too small to resolve clearly at 15 cm. The raw scattering intensity, $I_{raw}(q,L)$, was corrected for these changes and for background scattering and reported as $I(q)$,

$$I(q) = [I_{raw}(q,L) - I_{bgd}(q,L)](L^2/15^2) \qquad (1)$$

where $I_{bgd}(q,L)$ is the signal recorded from the disordered sample and L is the sample-to-screen distance in centimeters.

Experimental Data

The sample was disordered by heating to 70 °C and then quiescently quenched to a predetermined temperature, T, in the ordered state. We present data at four quench temperatures: 50.0, 52.0, 53.7, and 55.5 °C. Time zero ($t = 0$) is defined as the time at which the quench was initiated, and it took about 15 min for the sample temperature to reach equilibrium. No significant scattering was observed at quench temperatures of 56.5 °C and above, even waiting as long as 1000 min, suggesting that activation barriers for grain growth are quite high under these conditions.

In Figure 2 we show typical scattering data obtained at $T = 50.0$ °C and $t = 420$ min. We also show the signal from the disordered sample (uncorrected) for reference. At times less than 240 min, the measured scattering is indistinguishable from the disordered state signal. It is possible that the scattering from the grains during this time is not strong enough for detection. On the other hand, there may be an induction time associated with the nucleation of ordered grains

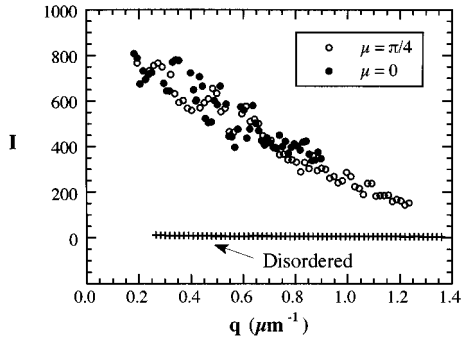

Figure 2. Depolarized scattering intensity data, I, versus q along $\mu = 0$ (filled circles) and $\mu = \pi/4$ (unfilled circles) directions at $t = 420$ min, obtained at 50.0 °C. The crosses represent data obtained in the disordered state (70 °C) which were independent of μ.

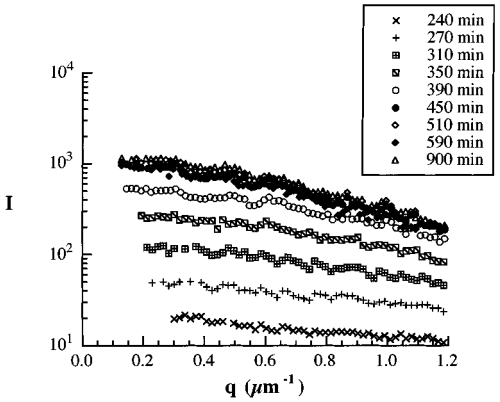

Figure 3. Development of the intensity profiles along $\mu = \pi/4$ with time obtained at 50.0 °C.

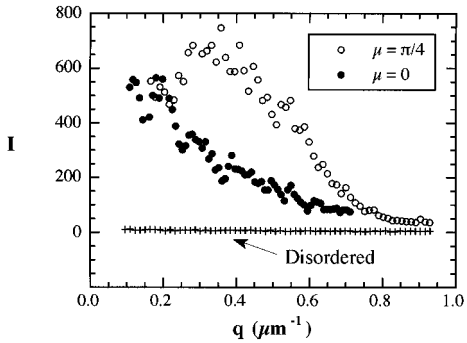

Figure 4. Depolarized scattering intensity data, I, versus q along $\mu = 0$ and $\mu = \pi/4$ directions at $t = 390$ min, obtained at 53.7 °C. The crosses represent data obtained in the disordered state (70 °C) which were independent of μ.

under these conditions. At $T = 50.0$ °C, we find that the scattering pattern is azimuthally symmetric and the scattering profiles along $\mu = 0$ and $\mu = \pi/4$ are the same, within experimental error (see Figure 2). In Figure 3 we show the time dependence of the scattering profiles at $T = 50.0$ °C. Only data along the $\mu = \pi/4$ direction are shown. The scattering intensity increases by 3 orders of magnitude during the ordering process. At intermediate times ($240 < t < 450$ min) the scattering profiles change rapidly, indicating a rapid growth of the ordered phase. However, the evolution of the scattering profiles slows down considerably after $t = 450$ min; the data obtained between $t = 450$ and 900 min are essentially indistinguishable.

In Figure 4 we show the scattering data obtained at $T = 53.7$ °C and $t = 390$ min. As always, the sample was disordered before this experiment was begun. It is evident that the scattering pattern under these conditions is azimuthally asymmetric. This asymmetry persists throughout the observable growth process at 53.7 °C. The scattering intensity along $\mu = \pi/4$ is much larger than that along $\mu = 0$. In addition, a scattering peak at $q = 0.35$ μm^{-1} is evident along the $\mu = \pi/4$ direction. The evolution of the scattering profiles at $T = 53.7$ °C along $\mu = \pi/4$ is shown in Figure 5, where we plot the logarithm of the scattering intensity versus q. We see no signal in the first 240 min, followed by a rapid increase in scattering intensity at times between 240 and 800 min. The scattering profiles at $t > 900$ min evolve slowly with time. The data at $t = 900$ and $t = 1140$ min are essentially superposable. In Figure 6 we show the time dependence of the scattering intensity along the $\mu = 0$ direction for the $T = 53.7$ °C quench. The trends are similar to those seen in Figure 5, except for the fact that the scattering intensity along the $\mu = 0$ direction is a monotonic function of q at all times. Results obtained at $T = 52.0$ °C were qualitatively similar to those obtained at $T = 53.7$ °C.

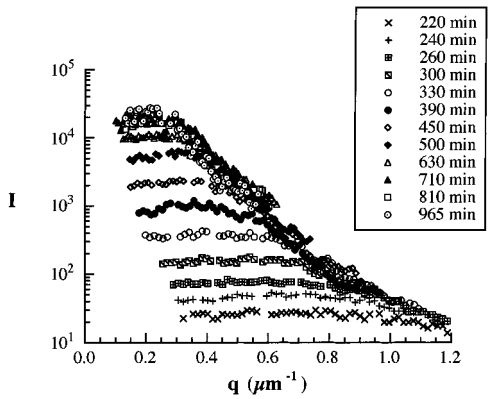

Figure 5. Development of intensity profiles along $\mu = \pi/4$ with time obtained at 53.7 °C.

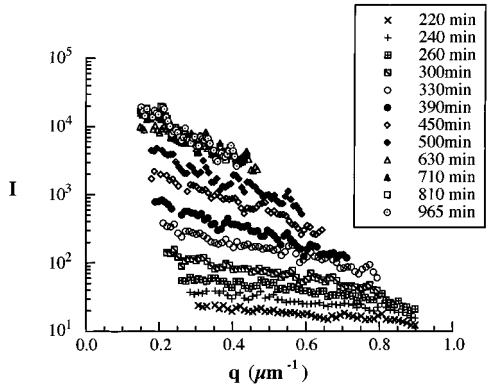

Figure 6. Development of intensity profiles along $\mu = 0$ with time obtained at 53.7 °C.

In Figure 7 we show typical scattering data at $T = 55.5$ °C. We find azimuthal asymmetry in the scattering pattern, but the scattering profiles along both $\mu = 0$ and $\mu = \pi/4$ are monotonically decreasing functions of q. The weak scattering maximum that was found along the $\mu = \pi/4$ direction at $T = 52.0$ and 53.7 °C is absent. In addition, the dependence of the scattering intensity at a given q on μ is weaker; compare Figure 7 with Figure 4, recorded at $t = 500$ and $t = 390$ min, respectively.

We have thus found three qualitatively different, depolarized light scattering patterns in the SI(4-13) sample: azimuthally symmetric scattering patterns at 50.0 °C, azimuthally asymmetric scattering patterns without scattering peaks at 55.5 °C, and azimuthally asymmetric scattering patterns with scattering peaks at 52.0 and 53.7 °C. In the next section we develop a theoretical framework which enables us to obtain quantitative information about the granular organization in SI(4-13) from these light scattering measurements.

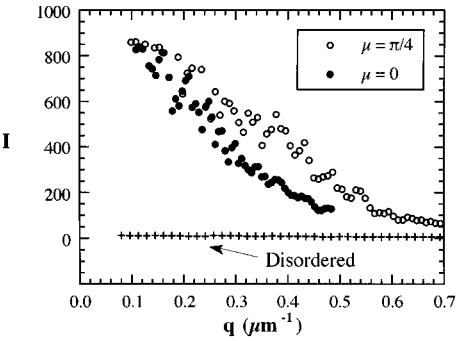

Figure 7. Depolarized scattering intensity data, I, versus q along $\mu = 0$ and $\mu = \pi/4$ directions at $t = 500$ min, obtained at 55.5 °C. The crosses represent data obtained in the disordered state (70 °C) which were independent of μ.

Theoretical Formulation

The theory presented here is aimed toward providing a model of grain organization that can account for the characteristic features of the scattering pattern, in particular, the off-axis maximum observed in the experimental plots of the scattering intensity versus the magnitude of the scattering vector. The sample is assumed to consist of a collection of uniaxial optically anisotropic grains with a rodlike shape, the optic axis of each grain being parallel to the rod axis. The ordinary and extraordinary refractive indices are n_o and n_e, respectively. The grains are taken to be organized into correlated clusters with mutually perpendicular grain axes. The relative orientation of the grains within each cluster is the same, but the orientation of the cluster varies randomly over the sample. We consider the cases of one, two, or three grains per cluster.

If there are n grains per correlated cluster, there are $n(n-1)/2$ grain pairs per cluster. The sample is made up of N clusters. The field, E_i, scattered from the input plane wave of amplitude E_o, by the ith cluster, to the far field point $\mathbf{r}_{ff}$, is

$$E_i = \frac{C}{r_{ff}} E_o \exp(-ikr_{ff}) \sum_{j=1}^{n} \mathbf{a}_x \cdot \mathbf{g}_{ij} \mathbf{g}_{ij} \cdot \mathbf{a}_y F_{ij}(\mathbf{q}) \qquad (2)$$

where $\{\mathbf{a}_x, \mathbf{a}_y\}$ are unit vectors in the direction of the {analyzer, polarizer}, $\mathbf{q}$ is the scattering vector, and $C = n(n_e - n_o)k^2/2\pi$. The far field point is represented by

$$\mathbf{r}_{ff} = r_{ff} (\sin\theta \sin\mu, \sin\theta \cos\mu, \cos\theta) \qquad (3)$$

The scattering vector will be approximated by its paraxial limit:

$$\mathbf{q} = k\theta(\sin\mu, \cos\mu, 0) \qquad (4)$$

The unit vector, $\mathbf{g}_{ij}$, is in the direction of the optic axis of the jth grain of the ith cluster, and $F_{ij}(\mathbf{q})$ is the Fourier transform of its shape factor:

$$F_{ij}(\mathbf{q}) = \int d\mathbf{r}' \, e^{-i\mathbf{q}\cdot\mathbf{r}'} f_{ij}(\mathbf{r}') \qquad (5)$$

where $f_{ij}(\mathbf{r}')$ is equal to 1 if $\mathbf{r}'$ lies in the grain and 0 otherwise. We note that in the case of forward scattering, when $\mathbf{q} = 0$, the transform equals the grain volume:

$$F_{ij}(0) = \mathrm{vol}_{ij} \qquad (6)$$

For a sample consisting of N uncorrelated clusters, the scattered intensity is given by

$$I_{\mathrm{scattered}}(\theta,\mu) = \frac{C^2}{\mathbf{r}_{ff}^2}\Big(\sum_{i=1}^{N}\Big[\sum_{j=1}^{n}(\mathbf{a}_x\cdot\mathbf{g}_{ij}\mathbf{g}_{ij}\cdot\mathbf{a}_y)^2|F_{ij}^2(\mathbf{q})| + \sum_{j=1}^{n}\sum_{k=1}^{j-1}(\mathbf{a}_x\cdot\mathbf{g}_{ij}\mathbf{g}_{ij}\cdot\mathbf{a}_y)(\mathbf{a}_x\cdot\mathbf{g}_{ik}\mathbf{g}_{ik}\cdot\mathbf{a}_y)(F_{ij}(\mathbf{q})\,F_{ik}^*(\mathbf{q}) + F_{ik}(\mathbf{q})\,F_{ij}^*(\mathbf{q}))\Big]\Big) \qquad (7)$$

Spatial Symmetry of Scattering Patterns. In the expressions for the scattered intensity, the only reference to the laboratory frame occurs in the terms $(\mathbf{a}_x\cdot\mathbf{g}_{ij}\mathbf{g}_{ij}\cdot\mathbf{a}_y)^2$ and $(\mathbf{a}_x\cdot\mathbf{g}_{ij}\mathbf{g}_{ij}\cdot\mathbf{a}_y)(\mathbf{a}_x\cdot\mathbf{g}_{ik}\mathbf{g}_{ik}\cdot\mathbf{a}_y)$. Each of these terms is invariant with respect to 90° rotations about the z axis, $\{\mathbf{a}_x \rightarrow -\mathbf{a}_y, \mathbf{a}_y \rightarrow \mathbf{a}_x\}$, and with respect to reflections in the $x-z$ plane, $\mathbf{a}_x \rightarrow \mathbf{a}_x, \mathbf{a}_y \rightarrow -\mathbf{a}_y\}$ and the $y-z$ plane, $\{\mathbf{a}_x \rightarrow -\mathbf{a}_x, \mathbf{a}_y \rightarrow \mathbf{a}_y\}$. Since, as will be seen below, the dependence on the azimuthal scattering angle, μ, is expressible as a Fourier series in the angle μ, with a maximum order of 4μ, these symmetry conditions imply that the dependence of the scattered intensity on the scattering angles is of the form

$$I_{\mathrm{scattered}}(\theta,\mu) \propto \alpha(\theta) + \beta(\theta)\cos(4\mu) \qquad (8)$$

Evaluation. Two types of terms enter, n terms from direct contributions from single grains and $n(n-1)/2$ cross-terms from the interference of grain pairs. To facilitate later evaluations, we approximate the grain shape functions by Gaussian forms whose contours of constant value are ellipsoids of revolution about the grain axis:

$$f_{ij}(\mathbf{r}) = \exp\left(-\left(\frac{\mathbf{g}_{ij}\cdot\mathbf{r}}{l_j}\right)^2\right)\exp\left(-\frac{(\mathbf{m}_{ij}\cdot\mathbf{r})^2 + (\mathbf{n}_{ij}\cdot\mathbf{r})^2}{w_j^2}\right) \qquad (9)$$

In this expression, the vector $\mathbf{r}$ is measured from the center of the grain and $(\mathbf{g}, \mathbf{m}, \mathbf{n})$ constitute an orthogonal set of unit vectors. In the expressions involving cross-terms both radius vectors must be referred to the same origin. Thus, if the above expression represents the shape factor for the jth grain, then, in an interference term involving the j and k grains, the k grain shape factor will be represented by

$$f_{ik}(\mathbf{r}) = \exp\left(-\left(\frac{\mathbf{g}_{ik}\cdot(\mathbf{r}-\mathbf{L}_{jk})}{l_j}\right)^2\right) \exp\left(-\frac{(\mathbf{m}_{ik}\cdot(\mathbf{r}-\mathbf{L}_{jk}))^2 + (\mathbf{n}_{ik}\cdot(\mathbf{r}-\mathbf{L}_{jk}))^2}{w_j^2}\right) \qquad (10)$$

where $\mathbf{L}_{jk}$ is a vector connecting the centers of grains j and k within a cluster. We have assumed that the grain shape parameters, l and w, while possibly different among the grains of a correlated cluster, are the same for the corresponding grains in different clusters. Since different clusters are assumed to be uncorrelated, we can evaluate the effect of a distribution of sizes among the different clusters by averaging the output over the assumed distribution. Using the Gaussian forms, the direct and cross-term contributions to the scattering intensity are

$$|F_{ij}{}^2(\mathbf{q})| = \pi^3(l_j w_j{}^2)^2 \exp\left(-\frac{w_j{}^2 q^2}{2}\right) \exp\left(-\frac{(l_j{}^2 - w_j{}^2)(\mathbf{q}\cdot\mathbf{g}_{ij})^2}{2}\right)$$

$$G_{ijk}(\mathbf{q}) \equiv F_{ij}(\mathbf{q})\, F_{ik}^*(\mathbf{q}) + F_{ik}(\mathbf{q})\, F_{ij}^*(\mathbf{q}) = 2\,\pi^3\,(l_j w_j{}^2)\,(l_k w_k{}^2)\cos(\mathbf{q}\cdot\mathbf{L}_{jk}) \exp\left(-\frac{(w_j{}^2 + w_k{}^2)\,q^2}{4}\right) \exp\left(-\frac{(l_j{}^2 - w_j{}^2)\,(\mathbf{q}\cdot\mathbf{g}_{ij})^2 + (l_k{}^2 - w_k{}^2)\,(\mathbf{q}\cdot\mathbf{g}_{ik})^2}{4}\right) \quad (11)$$

We characterize each grain cluster by the orientation angles, θ_1 and μ_1, of the grain axis of one grain of the cluster, arbitrarily called the "1" grain, and the spin angle, σ_1, about that axis. The orientations of the grain axes of the other grains of the cluster are defined relative to the 1-grain. The 1-grains of the different clusters point in different directions. Assuming a uniform distribution of orientations, the number of 1-grains with a differential orientation range characterized by the polar and spin angles of $\mathbf{g}_1$ is

$$\mathrm{d}N_1 = N \sin\theta_1\, \mathrm{d}\theta_1\, \mathrm{d}\mu_1\, \mathrm{d}\sigma_1/8\pi^2 \quad (12)$$

Introducing the notation

$$\frac{1}{8\pi^2}\int_0^{\pi} \sin\theta_1\, \mathrm{d}\theta_1 \int_0^{2\pi} \mathrm{d}\mu_1 \int_0^{2\pi} \mathrm{d}\sigma_1 \rightarrow \int \mathrm{d}\mathbf{g}_1 \quad (13)$$

the expression for the scattered intensity takes the form

$$I_{\mathrm{scattered}}(\theta,\mu) = (C^2 N I_{\mathrm{inc}}/r_{\mathrm{ff}}{}^2)\int \mathrm{d}\mathbf{g}_1 \Big(\sum_{j=1}^{n} (\mathbf{a}_x\cdot\mathbf{g}_j\mathbf{g}_j\cdot\mathbf{a}_y)^2 |F^2(\mathbf{q},\mathbf{g}_j,l_j,w_j)| + \sum_{j=1}^{n}\sum_{k=1}^{j-1} (\mathbf{a}_x\cdot\mathbf{g}_j\mathbf{g}_j\cdot\mathbf{a}_y)(\mathbf{a}_x\cdot\mathbf{g}_k\mathbf{g}_k\cdot\mathbf{a}_y) G(\mathbf{q},\mathbf{g}_j,\mathbf{g}_k,l_j,w_j,l_k,w_k,\mathbf{L}_{jk})\Big) \quad (14)$$

where I_{inc} is the incident light intensity. The θ and μ dependence of the right-hand side is contained implicitly in the scattering vector $\mathbf{q}$. The i subscript is suppressed since it is implicit in the $\mathbf{g}_1$ integral. The F, G notation has been modified to indicate the explicit dependence of the shape factor on the direction of the grain axis and grain shape parameters. In order to evaluate this integral, all of the angles used to describe the other grain axes in a cluster must be expressed in terms of those of the 1-grain. If $n = 1$, we use $\mathbf{g}_1$; if $n = 2$, we use $\mathbf{g}_1$ and $\mathbf{g}_2$; if $n = 3$, we use $\mathbf{g}_1$, $\mathbf{g}_2$, and $\mathbf{g}_3$, where

$$\mathbf{g}_1 = [\sin\theta_1 \sin\mu_1,\ \sin\theta_1 \cos\mu_1,\ \cos\theta_1\}$$

$$\mathbf{a}_x\cdot\mathbf{g}_1\mathbf{g}_1\cdot\mathbf{a}_y = (1/2)\sin^2\theta_1 \sin(2\mu_1)$$

$$\mathbf{a}_x\cdot\mathbf{g}_2\mathbf{g}_2\cdot\mathbf{a}_y = (1/2)\,(\cos\theta_1 \cos(2\mu_1)\sin(2\sigma_1) - \cos^2\sigma_1 \sin(2\mu_1) + \cos^2\theta_1 \sin^2\sigma_1 \sin(2\mu_1))$$

$$\mathbf{a}_x\cdot\mathbf{g}_3\mathbf{g}_3\cdot\mathbf{a}_y = (1/2)\,(-\cos\theta_1 \cos(2\mu_1)\sin(2\sigma_1) - \sin^2\sigma_1 \sin(2\mu_1) + \cos^2\theta_1 \cos^2\sigma_1 \sin(2\mu_1)) \quad (15)$$

$$\mathbf{q}\cdot\mathbf{g}_1 = q\cos(\mu_1 - \mu)\sin\theta_1$$

$$\mathbf{q}\cdot\mathbf{g}_2 = q(\cos\theta_1 \cos(\mu_1 - \mu)\sin\sigma_1 - \cos\sigma_1 \sin(\mu_1 - \mu))$$

$$\mathbf{q}\cdot\mathbf{g}_3 = q(\cos\theta_1 \cos(\mu_1 - \mu)\cos\sigma_1 + \sin\sigma_1 \sin(\mu_1 - \mu)) \quad (16)$$

Under the μ_1 integral, we may change the variable of integration to $\mu_1 + \mu$. This puts the dependence on μ in the coefficients of F and G, where it is of the form previously described, namely, a Fourier series in μ with a maximum order of 4μ. Thus, using the argument leading to (8), the expression for the scattered intensity may be written

$$I_{\mathrm{scattered}}(\theta,\mu) = (C^2 N I_{\mathrm{inc}}/r_{\mathrm{ff}}{}^2)\,(\sum_{j=1}^{n} I_{jj} + \sum_{j=1}^{n}\sum_{k=1}^{j-1} I_{jk}) \quad (17)$$

where we define I_{jj}, I_{jk}, α_{jj}, β_{jj}, α_{jk}, and β_{jk} by

$$I_{jj} = \int \mathrm{d}\mathbf{g}_1\, (\mathbf{a}_x\cdot\mathbf{g}_j\mathbf{g}_j\cdot\mathbf{a}_y)^2 |F^2(\mathbf{q},\mathbf{g}_j,I_j,w_j)| \equiv \alpha_{jj} + \beta_{jj}\cos(4\mu)$$

$$I_{jk} = \int \mathrm{d}\mathbf{g}_1 (\mathbf{a}_x\cdot\mathbf{g}_j\mathbf{g}_j\cdot\mathbf{a}_y) \times (\mathbf{a}_x\cdot\mathbf{g}_k\mathbf{g}_k\cdot\mathbf{a}_y) G(\mathbf{q},\mathbf{g}_j,\mathbf{g}_k,l_j,w_j,l_k,w_k,\mathbf{L}_{jk}) \equiv \alpha_{jk} + \beta_{jk}\cos(4\mu) \quad (18)$$

Forward Scattering. For the case of forward scattering, $\mathbf{q} = 0$, we have from (6) and (11)

$$F^2(0,\mathbf{g}_j,l_j,w_j) = \pi^3(l_j w_j{}^2)^2 = \mathrm{vol}_j{}^2$$

$$G(0,\mathbf{g}_j,\mathbf{g}_k,l_j,w_j,l_k,w_k,\mathbf{L}_{jk}) = 2\pi^3\,(l_j w_j{}^2)(l_k w_k{}^2) = 2\,\mathrm{vol}_j \mathrm{vol}_k \quad (19)$$

where vol_j is the volume of the jth grain and the forward scattered intensity is given by

$$I_{\mathrm{scattered}}(\theta = 0) = (C^2 N I_{\mathrm{inc}}/r_{\mathrm{ff}}{}^2)\,\pi^3 \int \mathrm{d}\mathbf{g}_1 \Big(\sum_{j=1}^{n} (\mathbf{a}_x\cdot\mathbf{g}_j\mathbf{g}_j\cdot\mathbf{a}_y)^2 (l_j w_j{}^2)^2 + 2\sum_{j=1}^{n}\sum_{k=1}^{j-1} (\mathbf{a}_x\cdot\mathbf{g}_j\mathbf{g}_j\cdot\mathbf{a}_y)(\mathbf{a}_x\cdot\mathbf{g}_k\mathbf{g}_k\cdot\mathbf{a}_y)\,(l_j w_j{}^2)(l_k w_k{}^2)\Big) \quad (20)$$

It is significant that for the special case where the basic cluster consists of three grains with the same shape and with mutually perpendicular axes, the forward scattering cross-section vanishes. This is because in that case the integrand in (20) is proportional to $(\mathbf{a}_x\cdot\sum_{j=1}\mathbf{g}_j\mathbf{g}_j\cdot\mathbf{a}_y)^2 = (\mathbf{a}_x\cdot\overleftrightarrow{\mathbf{I}}\cdot\mathbf{a}_y)^2$, which vanishes identically, where $\overleftrightarrow{\mathbf{I}}$ is the identity dyadic. More generally, we use the following expressions and integrals:

$$\mathbf{a}_x\cdot\mathbf{g}_1\mathbf{g}_1\cdot\mathbf{a}_y = (1/2)\sin^2\theta_1 \sin(2\mu_1)$$

$$\mathbf{a}_x\cdot\mathbf{g}_2\mathbf{g}_2\cdot\mathbf{a}_y = (1/2)(\cos\theta_1 \cos(2\mu_1)\sin(2\sigma_1) - \cos^2\sigma_1 \sin(2\mu_1) + \cos^2\theta_1 \sin^2\sigma_1 \sin(2\mu_1)) \quad (21)$$

$$\int d\mathbf{g}_1(\mathbf{a}_x\cdot\mathbf{g}_1\mathbf{g}_1\cdot\mathbf{a}_y)^2 = \frac{1}{8\pi^2}\int_0^\pi \sin\theta_1\, d\theta_1 \int_0^{2\pi} d\mu_1 \int_0^{2\pi} d\sigma_1\, ((1/2)\sin^2\theta_1 \sin(2\mu_1))^2 = {}^1/_{15}$$

$$2\int d\mathbf{g}_1\,(\mathbf{a}_x\cdot\mathbf{g}_1\mathbf{g}_1\cdot\mathbf{a}_y)(\mathbf{a}_x\cdot\mathbf{g}_2\mathbf{g}_2\cdot\mathbf{a}_y) = \frac{2}{8\pi^2}\int_0^\pi \sin\theta_1\, d\theta_1 \int_0^{2\pi} d\mu_1 \int_0^{2\pi} d\sigma_1\, ((1/2)\sin^2\theta_1 \sin(2\mu_1))$$

$$(1/2)(\cos\theta_1\cos(2\mu_1)\sin(2\sigma_1) - \cos^2\sigma_1\sin(2\mu_1) + \cos^2\theta_1\sin^2\sigma_1\sin(2\mu_1)) = -{}^1/_{15} \quad (22)$$

For single grain cells there is no cross-term,

$$I_{\text{scattered}}(\theta{=}0)|_{1\text{ grain}} = ({}^1/_{15}C^2NI_{\text{inc}}/r_{\text{ff}}{}^2)\,\text{vol}_1{}^2 \quad (23)$$

For two grain cells there is one cross-term:

$$I_{\text{scattered}}(\theta{=}0)|_{2\text{ grain}} = ({}^1/_{15}C^2NI_{\text{inc}}/r_{\text{ff}}{}^2)(\text{vol}_1{}^2 + \text{vol}_2{}^2 - \text{vol}_1\text{vol}_2) \quad (24)$$

If the two grains have the same volume, vol_1,

$$I_{\text{scattered}}(\theta{=}0)|_{2\text{ grain}} = ({}^1/_{15}C^2NI_{\text{inc}}/r_{\text{ff}}{}^2)(\text{vol}_1{}^2) \quad (25)$$

For three grain cells

$$I_{\text{scattered}}(\theta{=}0)|_{3\text{ grain}} = ({}^1/_{15}C^2NI_{\text{inc}}/r_{\text{ff}}{}^2)(\text{vol}_1{}^2 + \text{vol}_2{}^2 + \text{vol}_3{}^2 - \text{vol}_1\text{vol}_2 - \text{vol}_1\text{vol}_3 - \text{vol}_2\text{vol}_3)$$

$$= ({}^1/_{15}C^2NI_{\text{inc}}/r_{\text{ff}}{}^2){}^1/_2((\text{vol}_1 - \text{vol}_2)^2 + (\text{vol}_1 - \text{vol}_3)^2 + (\text{vol}_2 - \text{vol}_3)^2) \quad (26)$$

For the case where two of the three cells have the same volume, e.g. $\text{vol}_1 = \text{vol}_3$, we have

$$I_{\text{scattered}}(\theta{=}0)|_{3\text{ grain}} = ({}^1/_{15}C^2NI_{\text{inc}}/r_{\text{ff}}{}^2)(\text{vol}_1 - \text{vol}_2)^2 \quad (27)$$

As shown earlier, if all three grains have the same volume, the forward scattering vanishes.

Certain results apply to forward scattering even when we relax some of the grain model assumptions made to this point. If we allow there to be a distribution (i.e. a polydispersity) of grain sizes among the grain clusters and take averages over the distribution, we get, assuming that there is no statistical distinction between the grains,

$$I_{\text{scattered}}(\theta{=}0)|_{3\text{ grain}} = ({}^1/_{15}C^2NI_{\text{inc}}/r_{\text{ff}}{}^2)(\langle\text{vol}^2\rangle - \langle\text{vol}\rangle^2) \quad (28)$$

In appendix 2 and the section entitled "Fitting Procedure" we will also discuss the effect of non-orthogonality of grain axes on forward scattering.

Scattering at Finite Scattering Vectors. In general we are unable to get simple analytic expressions for the $\mathbf{g}_1$ integral, but results can be obtained in terms of one- and two-dimensional integrals that are evaluated numerically. In the following we will assume that all of the $\mathbf{L}_{ij}$ are parallel to $\mathbf{g}_1$. In appendix 1 we show, for the direct contribution from the grain j,

$$\begin{pmatrix}\alpha_{jj}\\ \beta_{jj}\end{pmatrix} = \frac{\pi^3(l_jw_j{}^2)^2}{16}\exp\left(-\frac{w_j{}^2q^2}{2}\right)\int_o^\pi d\theta_1\,\sin^5\theta_1\,\exp(-\kappa_j\sin^2\theta_1)\begin{pmatrix}I_0(\kappa_j\sin^2\theta_1)\\ I_2(\kappa_j\sin^2\theta_1)\end{pmatrix} \quad (29)$$

where I_m is the hyperbolic Bessel function of order m and where

$$\kappa_j = (q^2/4)(l_j{}^2 - w_j{}^2) \quad (30)$$

Depending on their relative orientation, there are many possible forms for the cross-term contributions from grains j and k. We will consider here two cases: the T configuration, where one grain is pointing toward the center of the other perpendicular grain, and the skew configuration, where the two perpendicular grains' axes lie in parallel planes. In both cases it is assumed that the grain centers are separated by the distance L_{jk} along the $\mathbf{g}_1$ axis, so we set $j = 1$. For the T configuration we have

$$\begin{pmatrix}\alpha_{1k}\\ \beta_{1k}\end{pmatrix}_{\text{T}} = \frac{\pi^2(l_1w_1{}^2)(l_kw_k{}^2)}{32}\exp\left(-\frac{q^2(w_1{}^2 + w_k{}^2) + 2\kappa_k}{4}\right)\int_o^\pi d\theta_1\,\sin^3\theta_1\int_0^{2\pi} d\mu_1\cos(qL_{1k}\sin\theta_1\cos\mu_1)\exp\left(-\left(\kappa_1 - \frac{\kappa_k}{2}\right)\cos^2\mu_1\sin^2\theta_1\right)\begin{pmatrix}H_\alpha\\ H_\beta\end{pmatrix}_{\text{T}} \quad (31)$$

where $k = 2$ or 3

$$\begin{pmatrix}H_\alpha\\ H_\beta\end{pmatrix}_{\text{T}} = \begin{pmatrix}a_\alpha\\ a_\beta\end{pmatrix}I_0\left(\frac{1}{2}\kappa_k\gamma\right) - \left(\begin{pmatrix}b_\alpha\\ b_\beta\end{pmatrix}\frac{\alpha}{\gamma} + \begin{pmatrix}c_\alpha\\ c_\beta\end{pmatrix}\frac{\beta}{\gamma}\right)I_1\left(\frac{1}{2}\kappa_k\gamma\right) \quad (32)$$

and

$$a_\alpha = -\sin^2\theta_1,\quad b_\alpha = -(1 + \cos^2\theta_1),\quad c_\alpha = 0$$

$$a_\beta = -\cos(4\mu_1)\sin^2\theta_1,\quad b_\beta = -\cos(4\mu_1)(1 + \cos^2\theta_1),\quad c_\beta = -2\sin(4\mu_1)\cos\theta_1$$

$$\alpha = \sin^2\mu_1 - \cos^2\mu_1\cos^2\theta_1,\quad \beta = \sin(2\mu_1)\cos\theta_1,\quad \gamma = (\alpha^2 + \beta^2)^{1/2} \quad (33)$$

For the skew configuration it is sufficient for our presentation to treat a special case where the two grains have the same shape. They are each perpendicular to $\mathbf{g}_1$, so we set $j = 2$, $k = 3$, $l_j = l_k = l$, $w_j = w_k = w$, and $\kappa_j = \kappa_k = \kappa$. Then

$$\begin{pmatrix}\alpha_{2,3}\\ \beta_{2,3}\end{pmatrix}_{\text{skew}} = \pm\frac{\pi^2}{128}(lw^2)^2e^{-(w^2q^2/2)}\int_0^\pi d\theta_1\,\sin\theta_1\int_0^{2\pi} d\mu_1\cos(2qL\sin\theta_1\cos\mu_1)\exp(-\kappa(\cos^2\theta_1\cos^2\mu_1 + \sin^2\mu_1))\begin{pmatrix}1 - 10\cos^2\theta_1 + \cos^4\theta_1\\ \cos(4\mu_1)\sin^4\theta_1\end{pmatrix} \quad (34)$$

One Grain per Cluster.

$$I_{\text{scattered}}(\theta,\mu)|_{1\text{ grain}} = (C^2NI_{\text{inc}}/r_{\text{ff}}{}^2)I_{11}(l,w) \quad (35)$$

For the special case where $l = w$, we have from (29)

$$I_{\text{scattered}}(\theta,\mu)|_{1\ \text{grain},l=w} = ({}^{1}/_{15}C^2NI_{\text{inc}}/r_{\text{ff}}{}^2)\pi^{1/2}w^6\exp(-q^2w^2/2) \quad (36)$$

Two Grains per Cluster.

T configuration: $\mathbf{L}_{12} = \mathbf{g}_1L$

$$I_{\text{scattered}}(\theta,\mu)|_{2\ \text{grain}} = (C^2NI_{\text{inc}}/r_{\text{ff}}{}^2)\,(I_{11}(l_1,w_1) + I_{11}(l_2,w_2) + I_{12,\text{T}}(l_1,w_1,l_2,w_2,L_{12})) \quad (37)$$

Three Grains per Cluster.

twisted-H configuration: $\mathbf{L}_{12} = -\mathbf{L}_{13} = \mathbf{g}_1L$, $\mathbf{L}_{23} = 2\mathbf{g}_1L$

$$I_{\text{scattered}}(\theta,\mu)|_{3\ \text{grain}} = (C^2NI_{\text{inc}}/r_{\text{ff}}{}^2)\,(I_{11}(l_1,w_1) + I_{11}(l_2,w_2) + I_{11}(l_3,w_3) + I_{12,\text{T}}(l_1,w_1,l_2,w_2,L_{12})) + I_{12,\text{T}}(l_1,w_1,l_3,w_3,L_{13})) + I_{23,\text{skew}}(l_2,w_2,l_3,w_3,L_{23})) \quad (38)$$

We have used the definitions

$$I_{jk,\text{T}} \equiv \alpha_{jk,\text{T}} + \beta_{jk,\text{T}}\cos(4\mu)$$

$$I_{jk,\text{skew}} \equiv \alpha_{jk,\text{skew}} + \beta_{jk,\text{skew}}\cos(4\mu) \quad (39)$$

We call the special case of twisted H where all L's are zero, 3D+. This case will be discussed in the next section. Figure 8 shows geometrical representations of the twisted-*H* and 3D+ configurations.

Fitting Procedure

The azimuthally symmetric 50.0 °C scattering data were least squares fit to a simple Gaussian function as described in eq 36, characterized by two parameters: a single length scale, w, and normalization [$I_{\text{scattered}}$ at $q = 0$]. A sample fit is shown in Figure 9.

The 55.5 °C profiles at $\mu = 0$ and $\mu = \pi/4$, which exhibited azimuthal asymmetry but no off-axis maxima, were simultaneously fit to a one-grain model using eq 35 with $I_{11} \equiv \alpha_{11} + \beta_{11}\cos(4\mu)$ as indicated by eq 17, getting α_{11} and β_{11} and from eqs 29 and 30 by setting $j = 1$. This model had three parameters: two length scales, l and w, and normalization. Sample fits are shown in Figure 10.

The 52.0 and 53.7 °C profiles both exhibited off-axis maxima, suggesting the presence of grain correlations and requiring the use of a multiple-grain model. For a three-grain model with identical grains, the theoretical intensity goes to zero at $q = 0$, in disagreement with experiment (see Figures 4 and 5). As discussed in the theory section, variation in grain volume within a cluster can account for nonzero scattering in the forward direction. This led us to modify both the twisted-H and 3D+ models by allowing grain 1 to be longer than grains 2 and 3: $l_1 = l_2(1 + \Delta) = l_3(1 + \Delta)$. This fourth parameter, Δ, allowed us better to fit the experimental forward scattered intensity and can be directly related to both the standard deviation in grain volume, δv, and the forward scattered intensity, $I_{\text{scattered}}(\theta{=}0)$ (eq 27):

$$\Delta^2 = 3(\delta v)^2/v^2 \quad (40)$$

$$I_{\text{scattered}}(\theta{=}0) = K\phi V_{\text{sample}}v\Delta^2/(3 + \Delta)^2 \quad (41)$$

where V_{sample} is the illuminated sample volume, ϕ is the volume fraction of the sample occupied by grains, K is an optical constant, and v is the average grain volume. The effect of Δ on the scattering profile is shown in the series of curves in Figure 11.

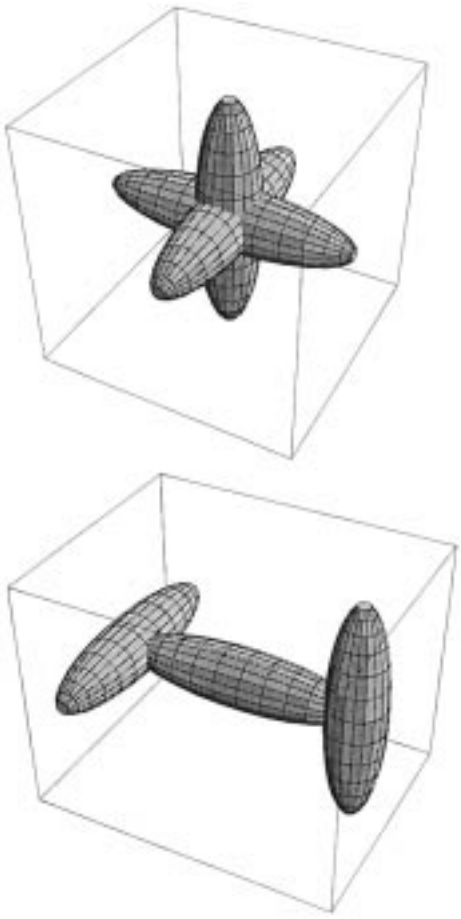

Figure 8. Geometrical representation of the three-grain 3D+ (a, top) and twisted-H (b, bottom) configurations.

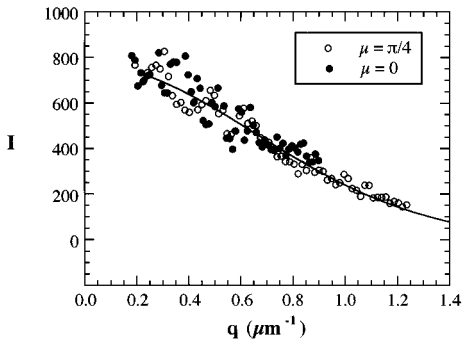

Figure 9. Least squares fit of experimental scattering profile at 50.0 °C, 420 min to the 1-grain model with single length scale, $w = 1.50$ μm.

We note that polydispersity in grain size is not the only factor that can account for nonzero scattering at $q = 0$ in the three-grain models; nonorthogonality of the three grains also results in finite forward scattering. Consider the three-grain twisted-H model with one leg turned through an angle $\Delta\sigma$. If we take the case of three grains with the same volume, the forward scattered intensity is given by (appendix 2)

$$I_{\text{scattered}}(\theta{=}0)|_{3\ \text{grain}} = ({}^{3}/_{15}C^2NI_{\text{inc}}/r_{\text{ff}}{}^2)(\text{vol}^2\sin^2\Delta\sigma_1) \quad (42)$$

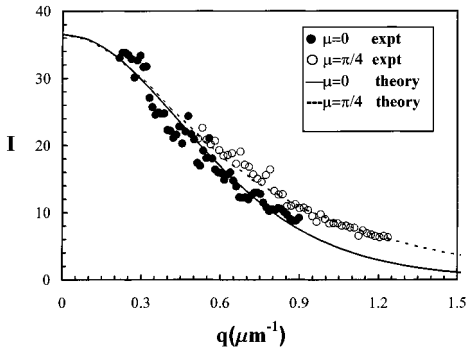

Figure 10. Least squares fit of experimental scattering profiles ($\mu = 0$ and $\mu = \pi/4$) at 55.5 °C, 305 min to the 1-grain model with two length scales, $w = 1.02$ μm, $l/w = 3$.

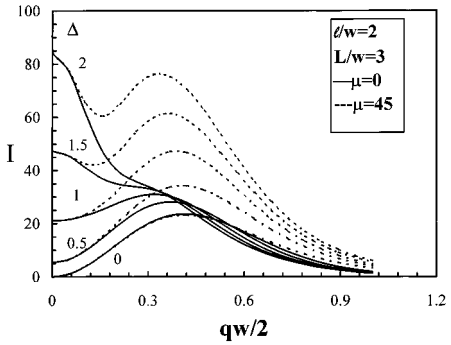

Figure 11. Effect of the polydispersity factor, Δ, on scattering profiles in the 3-grain twisted-H model.

Thus, the value of $\Delta\sigma$ that has the same effect on the forward scattering as Δ is given by the relation

$$\Delta^2 = 3 \sin^2 \Delta\sigma \qquad (43)$$

In Figure 12 we compare the experimentally measured scattering profiles at $T = 52.0$ °C and $t = 390$ min with the two-grain and three-grain cluster models. In the implementation of the two-grain T model and the three-grain twisted-H model, we always set L, the grain center spacing, equal to $l + w$. The theoretical results for the two-grain T model were obtained using eq 37, where I_{11} has the same form as for the one-grain case discussed above, and $I_{12,T} = \alpha_{12,T} + \beta_{12,T} \cos(4\mu)$, with $\alpha_{12,T}$ and $\beta_{12,T}$ obtained from eqs 31 and 30 with k set equal to 2. Both grains were assumed to have the same dimensions. Attempts to fit these data to a two-grain model were unsuccessful, as seen in Figure 12a.

Sample least squares fits of experimental data to the twisted-H and 3D+ models are shown in Figure 12b,c. The theoretical intensities for the twisted-H configuration can be obtained from eqs 38, 39, and 31−34. We assume that the 1 grain is the cross-bar of the twisted H. The form of I_{11} is the same as for the one-grain case discussed above. The values of $\{\alpha_{12,T}, \beta_{12,T}, \alpha_{23,skew}$, and $\beta_{23,skew}\}$which appear in (39), are obtained from eqs 31 and 34. The corresponding expressions for the 3D+ configuration are obtained by setting $L = 0$. In the three- and four-parameter least squares fits, the values of l/w were fit to the nearest 0.5 unit, and the values of Δ were fit to the nearest 0.25 unit. In all cases examined, the twisted-H model fit the experimental scattering profiles somewhat better, but not dramatically better, than the 3D+. That both models fit reasonably well is an indication of the robustness of the general three-grain cluster model. The sum of the

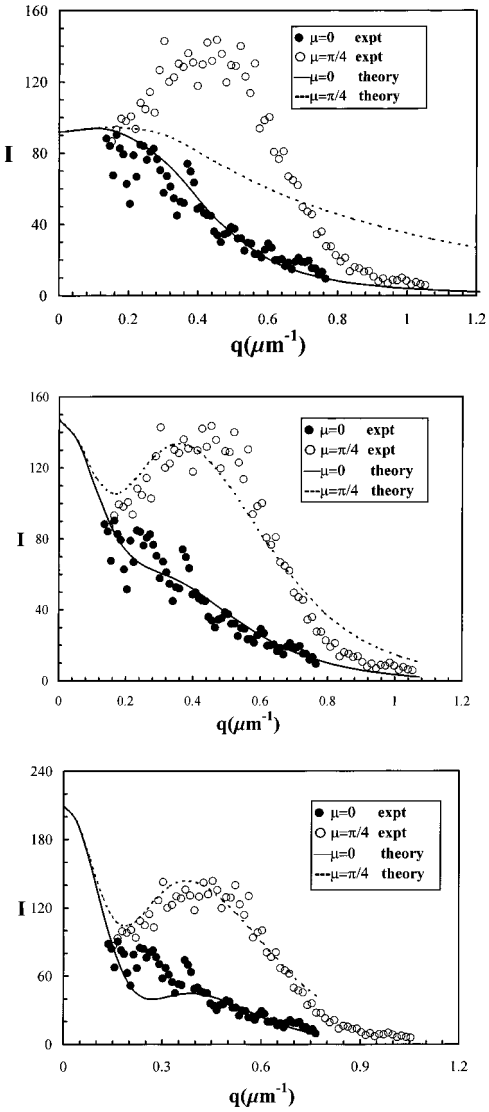

Figure 12. Least squares fits of experimental scattering profiles ($\mu = 0$ and $\mu = \pi/4$) at 52.0 °C, 390 min to the (a, top) 2-grain model ($w = 0.679$ μm, $l/w = 10$) and 3-grain models, (b, middle) twisted-H ($w = 1.86$ μm, $l/w = 2$, $\Delta = 2$), and (c, bottom) 3D+ ($w = 2.61$ μm, $l/w = 2$, $\Delta = 1$).

squares of the deviation between theory and experiment was lower in the twisted-H case by about 20%. In addition, the grain sizes obtained from the 3D+ fit had low aspect ratios (l/w) which imposes the unphysical condition that the three grains are overlapping over a substantial portion of their volume. We therefore only present least squares fits of the 52.0 and 53.7 °C data to the twisted-H model. The quality of the fits at all times was similar to that shown in Figure 12b. This is remarkable, given the small number of parameters and the elementary nature of the model. Even in simple, disordered systems, with a single correlation length, different functional forms are often required to fit low-q and high-q data.[23]

Evolution of Grain Structure. 50.0 °C. Analysis of light scattering profiles at different times (shown in Figure 3) allows us to follow the evolution of grain growth.[24] Structural changes occurring at $t < 240$ min could not be measured due to lack of a signal. After this early stage, we observe a period of rapid grain growth. However, the grains essentially stop growing after 600 min, reaching a plateau at $w = 1.7$ μm. The

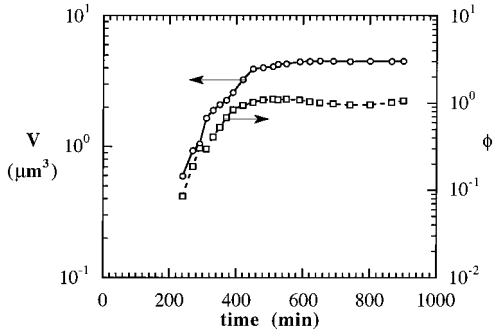

Figure 13. Time dependence of grain volume, v, and volume fraction occupied by grains, ϕ, at 50.0 °C.

grain structure remains ideal throughout their growth; i.e., there are no correlations between shape and the optic axis of the grains and no correlated clusters.

For the one-grain model employed at 50.0 °C, eq 23 for the forward scattered intensity can be written

$$I_{\text{scattered}}(\theta=0) = K\phi V_{\text{sample}} v \qquad (44)$$

$I_{\text{scattered}}(\theta=0)$ (or $I(0)$ for short) was estimated by evaluating the theoretically fitted intensity at $q = 0$. The grain volume, v, is proportional to w^3, so that a plot of $I(0)/w^3$ is equal to ϕ, the volume fraction of sample occupied by grains, multiplied by a constant that depends only on the geometrical configuration of the experiment. Both w^3 and $I(0)/w^3$ are plotted as a function of time in Figure 13. We see that both quantities level off to a constant value after 600 min. At long times, we expect the entire sample to be occupied by grains; i.e., $\phi \rightarrow 1$ as $t \rightarrow \infty$. In an earlier study on order formation in a polystyrene-*block*-polyisoprene copolymer, we found, using electron microscopy, that, at sufficiently long time, the entire sample was occupied by ordered grains.[17] It is difficult to imagine a mechanism by which ϕ in a one-component system would asymptotically approach a value that was different from unity, except perhaps in confined systems, where the presence of strain energy and surface effects might inhibit complete ordering. We therefore conclude that ϕ has leveled off at unity after $t = 600$ min. The proportionality constant in eq 44 was estimated by assuming that $\phi = 1$ for $t > 600$ min. At times less than 400 min we see that both v and ϕ increase with time. Note that these two quantities are estimated from independent measurements. The grain volume, v, is obtained from the angular distribution of the scattering light and is not affected by the absolute intensity. The grain volume fraction, ϕ, on the other hand, is directly proportional to the absolute intensity. At $t = 240$ min, when the depolarized light scattering signal rises significantly above the background, about 8% of the sample volume is occupied by ordered grains. It is thus evident that, in the first 450 min, the ordered grains coexist with the disordered phase. This implies that the phase transition mechanism for order formation in SI(4-13) at 50 °C is nucleation and growth. Ordered nuclei, formed during the early stages of the phase separation, grow at the expense of the disordered phase, and at $t = 450$ min, the entire sample is occupied by ordered grains. The disorder-to-order transformation is thus complete at this point. However, the grains, which now are in contact with each other via grain boundaries and other defects (point and line defects) can, in principle, continue to grow by defect annihilation. In SI(4-13) at 50 °C we see no evidence of this; there is no detectable increase in the grain volume, v, at times greater than 450 min. It is evident that kinetic barriers prevent defect annihilation under these conditions. This may be anticipated due to the proximity of the quench temperature to the glass transition temperature of the sample.

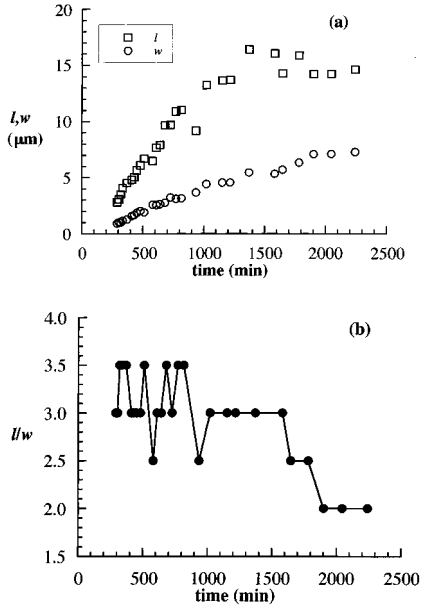

Figure 14. Time dependence of (a) grain size parameters, l and w, and (b) l/w at 55.5 °C.

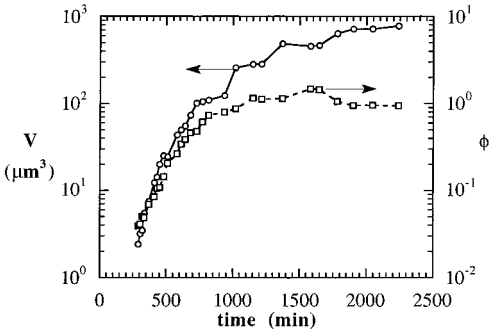

Figure 15. Time dependence of grain volume, v, and volume fraction occupied by grains, ϕ, at 55.5 °C.

55.5 °C. In Figures 14 and 15 we show data obtained at 55.5 °C where we see evidence for the formation of ellipsoidal grains, with characteristic lengths, l and w. In Figure 14a we plot l and w as a function of time, and in Figure 14b we plot the ratio l/w vs time. We see that at early times ($300 < t < 1000$ min), both l and w increase with time. However, there is no systematic change in the ratio l/w, which fluctuates about a mean value of 3. In this time window, we thus observe the growth of elongated grains whose average aspect ratio is conserved. A possible explanation for the anisotropic grain shape is that the interfacial tension between the sides of the cylinders and the disordered phase is less than that between the ends of the cylinders and the disordered phase. This is qualitatively consistent with recent theoretical calculations of Netz et al.[25] Note that anisotropy of grain shape was not found at 50.0 °C. This may be due to kinetic and/or thermodynamic factors. It is conceivable that the inequality of interfacial tensions along different directions within the growing grains diminishes with increasing quench depth and this

results in a loss of correlation between grain shape and the optic axis. On the other hand, the lower mobility of the chains at 50.0 °C may prevent the equilibrium grain structure from being attained and this could also lead to a loss of intragrain correlations.

A qualitative change in the grain growth occurs after about 1000 min. The growth rate of both l and w decreases, while the ratio l/w starts to drop, falling to a value of about 2. Equation 44 for the forward scattered intensity also applies at 55.5 °C, except that the average grain volume is proportional to the product lw^2, so that a plot of $I(0)/lw^2$ is proportional to ϕ. Both lw^2 and $I(0)/lw^2$ are plotted as a function of time in Figure 15. The ratio $I(0)/lw^2$ levels off to a constant value after about 1000 min, corresponding to $\phi = 1$, as was the case at 50.0 °C. However, the grain volume continues to increase beyond this point. We thus see evidence of grain growth after the entire sample is occupied by grains. This implies that there are two stages of grain growth in SI(4-13) at 55.5 °C: an early stage where grains grow at the expense of the disordered phase (t < 1000 min), and a late stage were grains grow by defect annihilation (t > 1000 min). This is qualitatively different from the observations at 50.0 °C, where grain growth by defect annihilation was not observed. The increased mobility at 55.5 °C relative to 50.0 °C is enough to overcome the kinetic barriers that prevented defect annihilation at 50.0 °C. However, the grain growth by defect annihilation occurs along a specific direction. The major axis of the grains, l, remains constant during this growth stage, and only the minor axis, w, increases with time, as seen in Figure 14a. This leads to a reduction in the ratio l/w seen in Figure 14b. The defect annihilation thus results in a loss of the intragrain correlations that were produced during the early stages of grain growth under these conditions. The ellipsoidal grains, which were presumably optimal structures when the grains were in contact with the disordered phase, may not be optimal after the entire sample is occupied by grains. High free energy defects are created at the boundaries between the space-filling grains. Grains that are spherical, on average, would have the least density of grain boundaries per unit volume. This appears to be the driving force for defect annihilation seen in SI(4-13) at 55.5 °C.

52.0 and 53.7 °C. Figures 16 and 17 describe the grain growth at 52.0 °C. At these temperatures we observed off-axis scattering maxima which are indicative of the presence of three-dimensionally correlated grain clusters. The grain parameters were obtained by applying the twisted-H model to the measured scattering patterns at all times. At 52.0 °C we see that both l and w increase at early times and then saturate at 6.5 and 4.5 μm. During this time there is little change in the grain anisotropy, l/w, and the polydispersity parameter, Δ, as is evident in Figure 16b. Using eq 41, we see that the quantity $[I(0)(3 + \Delta)^2/v\,\Delta^2]$ is proportional to ϕ, where $v = lw^2(3 + \Delta)/3$. Plots of v and ϕ vs time at 52.0 °C are shown in Figure 17. These data are similar to those obtained at 50 °C. We see an early growth process where grains grow at the expense of the disordered phase but no growth after the entire sample is occupied by grains ($\phi = 1$). The evolution of grain structure at 53.7 °C is qualitatively identical to that observed at 52.0 °C. We find that kinetic barriers prevent grain growth at 52.0 and 53.7 °C, in spite of the fact that these temperatures are above the measured glass transition temperature of the sample. We thus see evidence for the absence of defect annihilation in both glassy and rubbery regimes.

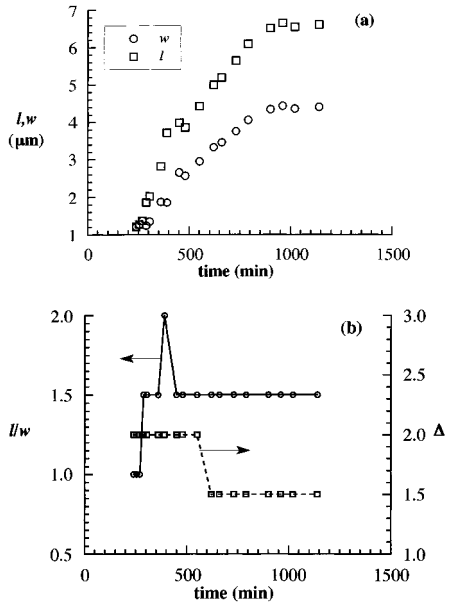

Figure 16. Time dependence of (a) grain size parameters, l and w, and (b) l/w and Δ at 52.0 °C.

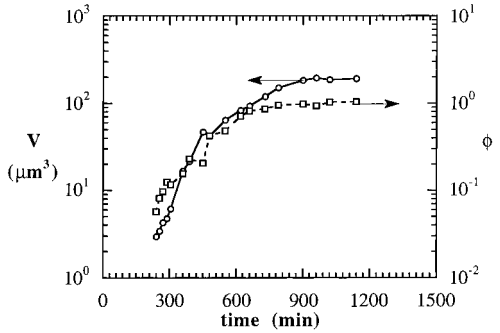

Figure 17. Time dependence of grain volume, v, and volume fraction occupied by grains, ϕ, at 52.0 °C.

Concluding Remarks

We have conducted a systematic study of ordering kinetics after quenching a block copolymer melt from the disordered state to the ordered state. We have obtained quantitative information about the size, shape, concentration, and correlations of ordered grains, as the transformation from disorder to order proceeds, by depolarized light scattering measurements. This information cannot be obtained from more conventional probes of block copolymer structure such as small-angle X-ray and neutron scattering, and rheology.[4−10] The material used in this study was a polystyrene-*block*-polyisoprene melt which exhibited a cylindrical microstructure at temperatures below 59 °C and a disordered phase at temperatures above 59 °C. Ordering kinetics were studied at temperatures ranging from 58 to 50 °C; the lower limit corresponds to the glass transition temperature, measured by DSC. At temperatures greater than 55.5 °C, no signatures of ordering were observed in the experimental time window, which was typically 10^3 min. At lower temperatures, we observed clear signatures of the ordering process and the depolarized light scattering intensity increased by several orders of magnitude. The ordering was carried out

Table 1. Summary of Grain Growth in SI(4-13)

T (°C)	grain structure	crossover time (min)	ζ	γ	l(steady) (μm)	w(steady) (μm)
50.0	1-grain isotropic	400	2.3	0.0	1.7	1.7
52.0	3-grain cluster ellipsoidal	600	4.1	0.1	6.5	4.5
53.7	3-grain cluster ellipsoidal	600	3.6	*a*	6.5	4.5
55.5	1-grain ellipsoidal	1000	3.9	1.6	15	7

[a] Not enough data taken to estimate exponent.

under quiescent conditions, and we therefore obtained a globally isotropic arrangement of ordered grains. However, in most of the experiments, the scattering patterns were azimuthally asymmetric, indicating the presence of local intragrain and intergrain correlations. A major undertaking in this project was the development of a unified theoretical framework for relating depolarized light scattering patterns to granular organization. Our conclusions regarding the evolution of grain structure are based on this model. The present work supercedes our earlier correlated grain-pair model, which was restricted to a limited set of grain-pair geometries and could not adequately describe the observed scattering profiles.[18]

We find that grain growth at all temperatures proceeds along certain common lines. This is demonstrated in Table 1, where we summarize our results on grain evolution in SI(4-13). Three regimes of grain growth are evident. At very early times (t < 200−300 min, depending on quench depth) we see no enhancement of the depolarized light scattering signal. Therefore, the structural evolution during this time cannot be probed directly. This is followed by a regime of rapid grain growth during which the volume fraction occupied by grains, ϕ, increases from about 0.05 to 1.0. The granular organization during this time was a strong function of temperature, as evidenced by qualitative changes in the depolarized light scattering profiles. We find that ordering proceeds via the formation of individual grains (50.0 and 55.5 °C) or the formation of correlated grain clusters (52.0 and 53.7 °C). The correlations within the clusters give rise to off-axis scattering peaks. We found that the scattering profiles from correlated clusters of two grains, which are necessarily two-dimensional clusters, were qualitatively inconsistent with the experimental data at 52.0 and 53.7 °C. The simplest grain model that was consistent with our data consisted of three-dimensional grain clusters comprising three mutually orthogonal (or nearly so) grains. Our experiments therefore indicate that under some conditions [quench temperatures between 52 and 53.7 °C for SI(4-13)] there is a tendency to obtain grain boundaries that are the junctions of mutually orthogonal cylinders. The only published study of the morphology of grain boundaries in cylindrical block copolymers that we are aware of,[26] in fact, shows precisely this kind of a grain boundary. The early processes leading to the formation of 3-grain clusters have not been identified. Perhaps the initial nucleation process resulted in the formation of one grain, and the other grains contained in the cluster were the result of secondary nucleation on the surface of the primary grain.

The regime of rapid grain growth is followed by a regime of extremely slow (or no detectable) grain growth, and we refer to it as the defect annihilation regime. The crossover times from growth to defect annihilation are estimated from the semilog plots of ϕ vs time (Figures 13, 15, and 17) and are given in Table 1. This crossover time increases with increasing quench depth, from 400 min at 50.0 °C to 1000 min at 55.5 °C. The fact that the growth is slowing down in spite of increasing temperature, is an indication of critically slowed growth kinetics.[11] The time dependence of the grain volume, v, was approximated by power laws[27] in the growth and defect annihilation regimes with exponents ζ and γ, respectively, and these values are given in Table 1. Finite grain growth rates in the defect annihilation regime (nonzero values of γ) were only observed at 55.5 °C. It is evident that the grain mobility at the lower temperatures is too low for detectable defect annihilation at the lower temperatures. At these low temperatures (<55.5 °C), the grain parameters l and w appear to approach steady state values at long times. These values are also given in Table 1. In the case of 55.5 °C only l approaches a steady state; the value of w reported in this case corresponds to the last measurement (t = 2250 min). It is evident that these steady state grain parameters increase monotonically with decreasing quench depth.

Knowledge of the kinetics of order formation is important for designing experiments that are aimed at determining the equilibrium phase diagram of block copolymer melts.[1] One has to ensure that the samples have been annealed for a sufficient amount of time so that the equilibrium morphology is achieved. In our experiments, we find that the conversion of disorder to order in SI(4-13) requires 400−1000 min, depending on quench depth. These experiments were conducted on an unentangled block copolymer melt with a longest relaxation time of about 1 s (based on rheology in the disordered state but close to the order-to-disorder transition). The time scales on which ordering takes place in SI(4-13) are several orders of magnitude slower, due to thermodynamic factors. Recent work by Goveas and Milner provides the framework for analyzing our experimental data in terms of these factors.[13] We will address these issues in a future publication[28] in the hope of gaining further insight into the factors that govern grain growth in block copolymers. It is important to note that, even in the most widely studied system, namely, crystalline solids, a comprehensive understanding of the factors that govern grain growth does not exist.[29]

Acknowledgment. We gratefully acknowledge financial support by the National Science Foundation (Grant No. DMR-9457950), Research Corp., and the donors of the Petroleum Research Fund, administered by the American Chemical Society, and we thank Jacqueline Goveas and Mohan Srinivasarao for useful discussions. We thank Dave Pine for his help in the design of the light scattering apparatus.

Appendix 1

Scattering Contribution from Random Ellipsoidal Grain. Since we average over all possible angles,

the contribution to $\{\alpha_{jj},\beta_{jj}\}$ from any grain has the same form, possibly differing only in the values of l_j and w_j. Thus, we may calculate the form of these expressions for any j by using the expressions appropriate for $j = 1$. We take the case $j = 1$ in expression 18 for I_{jj} and substitute from (11), (15), and (16) for $|F_{11}^2(\mathbf{q})|$, $\mathbf{a}_x\cdot\mathbf{g}_1\mathbf{g}_1\cdot\mathbf{a}_y$ and $\mathbf{q}\cdot\mathbf{g}_1$. Under the μ_1 integral, we change the variable of integration to $\mu_1 + \mu$. We may then identify α_{jj} and β_{jj} as the coefficients of the constant and $\cos(4\mu)$ terms. All other terms vanish under the angular integral, and we get

$$\begin{pmatrix}\alpha_{jj}\\ \beta_{jj}\end{pmatrix} = \frac{\pi^2(l_j w_j^2)^2}{32}\exp\left(-\frac{w_j^2 q^2}{2}\right)\int_0^\pi d\theta_1 \sin^5\theta_1 \exp(-\kappa_j \sin^2\theta_1)\int_0^{2\pi} d\mu_1 \begin{pmatrix}\exp[-(\kappa_j \sin^2\theta_1)\cos(2\mu_1)]\\ \cos(4\mu_1)\exp[-(\kappa_j \sin^2\theta_1)\cos(2\mu_1)]\end{pmatrix} \quad (A1.1)$$

Using the Fourier−Bessel integral for the hyperbolic Bessel function

$$I_m(z) = \frac{(-1)^m}{2\pi}\int_0^{2\pi} d\mu_1\, e^{-z\cos(\mu_1)}\cos(m\mu_1) \quad (A1.2)$$

we arrive at eq 29.

In contrast to the situation for the direct contribution, in the twisted-H configuration there are two nonequivalent configurations that contribute to the cross-terms. We call the cross-bar of the twisted H the 1 grain and assume that $\mathbf{L}_{23} = -2\mathbf{L}_{12} = 2\mathbf{L}_{13}$ is parallel to the $\mathbf{g}_1$ axis. We also assume that the 2 and 3 grains have the same dimensions. When we average over all angles, the $\{\alpha_{12},\beta_{12}\}$ and $\{\alpha_{13},\beta_{13}\}$ terms are equivalent and correspond to the T configuration of the 2-grain case, but the $\{\alpha_{23},\beta_{23}\}$ is not equivalent to the other two as it corresponds to a skew configuration.

To treat the T configuration we take the case $j = 1$, $k = 2$ in expression 18 for I_{jk} and substitute from (11), (15), and (16) for $G(\mathbf{q},\mathbf{g}_j,\mathbf{g}_k,l_j,w_j,l_k,w_k,\mathbf{L}_{jk})$, $(\mathbf{a}_x\cdot\mathbf{g}_j\mathbf{g}_j\cdot\mathbf{a}_y)(\mathbf{a}_x\cdot\mathbf{g}_k\mathbf{g}_k\cdot\mathbf{a}_y)$, and $\mathbf{q}\cdot\mathbf{g}_1,\mathbf{q}\cdot\mathbf{g}_2$. Following the same procedure as above to select the coefficients of the constant and $\cos(4\mu)$ terms, we get eq 31 with

$$\begin{pmatrix}H_\alpha\\ H_\beta\end{pmatrix} = \int_0^{2\pi} d\sigma_1 \left\{\begin{pmatrix}a_\alpha\\ a_\beta\end{pmatrix} + \begin{pmatrix}b_\alpha\\ b_\beta\end{pmatrix}\cos\left(2\sigma_1 + \begin{pmatrix}c_\alpha\\ c_\beta\end{pmatrix}\sin(2\sigma_1)\right)\right\} \exp\left(-\frac{1}{2}\kappa\{\alpha\cos(\sigma_1) + \beta\sin(\sigma_1)\}\right) \quad (A1.3)$$

with the coefficients given by (33). We get (32) by reexpressing the argument of the exponential using

$$\alpha\cos(2\sigma_1) + \beta\sin(2\sigma_1) = \gamma\cos(2\sigma_1 - \delta)$$

and using the generalization of (A1.2) when $\mu_1 \rightarrow \mu_1 - \phi$.

To treat the skew configuration, we take the case $j = 2$, $k = 3$ in expression 18 for I_{jk} and substitute from (11), (15), and (16) for $G(\mathbf{q},\mathbf{g}_j,\mathbf{g}_k,l_j,w_j,l_k,w_k,\mathbf{L}_{jk})$, $(\mathbf{a}_x\cdot\mathbf{g}_j\mathbf{g}_j\cdot\mathbf{a}_y)(\mathbf{a}_x\cdot\mathbf{g}_k\mathbf{g}_k\cdot\mathbf{a}_y)$, and $\mathbf{q}\cdot\mathbf{g}_1,\mathbf{q}\cdot\mathbf{g}_2$. Following the same procedure as above to select the coefficients of the constant and $\cos(4\mu)$ terms, we get eq 34 directly for the case in which the two grains of the pair are identical.

Appendix 2

Effect of Nonorthogonality for the Three-Grain Geometry. When we replace σ_1 in expressions involving $\mathbf{g}_2$ by $\sigma_1 + \Delta\sigma$ representations of $\mathbf{q}\cdot\mathbf{g}_2$ and $\mathbf{q}\cdot\mathbf{g}_3$ become

$$\mathbf{q}\cdot\mathbf{g}_2 = q(\cos\theta_1\cos(\mu_1 - \mu)\sin(\sigma_1 + \Delta\sigma_1) - \cos(\sigma_1 + \Delta\sigma_1)\sin(\mu_1 - \mu))$$

$$\mathbf{q}\cdot\mathbf{g}_3 = q(-\cos\theta_1\cos(\mu_1 - \mu)\cos(\sigma_1) + \sin(\sigma_1)\sin(\mu_1 - \mu)) \quad (A2.1)$$

The cross-term involving grains 1 and 2 is unchanged because they remain orthogonal:

$$2\int d\mathbf{g}_1(\mathbf{a}_x\cdot\mathbf{g}_1\mathbf{g}_1\cdot\mathbf{a}_y)(\mathbf{a}_x\cdot\mathbf{g}_2\mathbf{g}_2\cdot\mathbf{a}_y) = \frac{2}{8\pi^2}\int_0^\pi \sin\theta_1\, d\theta_1 \int_0^{2\pi} d\mu_1 \int_0^{2\pi} d\sigma_1\,((1/2)\sin^2\theta_1\sin(2\mu_1))$$

$$(1/2)(\cos\theta_1\cos(2\mu_1)\sin(2\sigma_1 + 2\Delta\sigma_1) - \cos^2(\sigma_1 + \Delta\sigma_1)\sin(2\mu_1) + \cos^2\theta_1\sin^2(\sigma_1 + \Delta\sigma_1)\sin(2\mu_1)) = -{}^1/_{15} \quad (A2.2)$$

The cross-term involving grains 2 and 3 becomes

$$2\int d\mathbf{g}_1\,(\mathbf{a}_x\cdot\mathbf{g}_2\mathbf{g}_2\cdot\mathbf{a}_y)(\mathbf{a}_x\cdot\mathbf{g}_3\mathbf{g}_3\cdot\mathbf{a}_y) = \frac{2}{8\pi^2}\int_0^\pi \sin\theta_1\, d\theta_1 \int_0^{2\pi} d\mu_1 \int_0^{2\pi} d\sigma_1$$

$$(1/2)(\cos\theta_1\cos(2\mu_1)\sin(2\sigma_1 + 2\Delta\sigma_1) - \cos^2(\sigma_1 + \Delta\sigma_1)\sin(2\mu_1) + \cos^2\theta_1\sin^2(\sigma_1 + \Delta\sigma_1)\sin(2\mu_1))$$
$$(1/2)(-\cos\theta_1\cos(2\mu_1)\sin(2\sigma_1) - \sin^2\sigma_1\sin(2\mu_1) + \cos^2\theta_1\cos^2\sigma_1\sin(2\mu_1)) = -{}^1/_{15} + (1/5)\sin^2(\Delta\sigma_1) \quad (A2.3)$$

We get for the scattering intensity

$$I_{\text{scattered}}(\theta{=}0)|_{3\text{ grain}} = ({}^3/_{15}C^2 N I_{\text{inc}}/r_{\text{ff}}^2)(\text{vol}_1^2 + \text{vol}_2^2 + \text{vol}_3^2 - \text{vol}_1\text{vol}_2 - \text{vol}_1\text{vol}_3 - \text{vol}_2\text{vol}_3(1 - 3\sin^2\Delta\sigma_1)) \quad (A2.4)$$

If we assume the three volumes are equal, we get eq 42.

References and Notes

(1) Bates, F. S.; Fredrickson, G. H. *Annu. Rev. Phys. Chem.* **1990**, *41*, 525.
(2) de Gennes, P. G.; Prost, J. *The Physics of Liquid Crystals*, 2nd ed.; Clarendon Press: Oxford, England, 1993.
(3) Seul, M.; Andelman, D. *Science* **1995**, *267*, 476.
(4) Harkless, C. R.; Singh, M. A.; Nagler, S. E.; Stephenson, G. B.; Jordan-Sweet, J. L. *Phys. Rev. Lett.* **1990**, *64*, 2285.
(5) Stuhn, B.; Vilesov, A.; Zachmann, H. G. *Macromolecules* **1994**, *27*, 3560.
(6) Floudas, G.; Fytas, G.; Hadjichristidis, N.; Pitsikalis, M. *Macromolecules* **1995**, *28*, 2359.
(7) Hashimoto, T.; Sakamoto, N. *Macromolecules* **1995**, *28*, 4779.
(8) Floudas, G.; Vlassopoulo, D.; Pitsikalis, M.; Hadjichristidis, N.; Stamm, M. *J. Chem. Phys.* **1996**, *104*, 2083.
(9) Rosedale, J. H.; Bates, F. S. *Macromolecules* **1990**, *23*, 2329.
(10) Winter, H. H.; Scott, D. B.; Gronski, W.; Okamoto, S.; Hashimoto, T. *Macromolecules* **1993**, *26*, 7236.
(11) Fredrickson, G. H.; Binder, K. *J. Chem. Phys.* **1989**, *91*, 7265.
(12) Qi, S.; Wang, Z. G. *Phys. Rev. Lett.* **1996**, *76*, 1679.
(13) Goveas, J. L.; Milner, S. T. *Macromolecules* **1997**, *30*, 2605.
(14) Fraaije, J. G. E. M. et al.; *J. Chem. Phys.* **1997**, *106*, 4260.
(15) Balsara, N. P.; Garetz, B. A.; Dai, H. J. *Macromolecules* **1992**, *25*, 6072.

(16) Garetz, B. A.; Newstein, M. C.; Dai, H. J.; Jonnalagadda, S. V.; Balsara, N. P. *Macromolecules* **1993**, *26*, 3151.
(17) Garetz, B. A.; Balsara, N. P.; Dai, H. J.; Wang, Z.; Newstein, M. C.; Majumdar, B. *Macromolecules* **1996**, *29*, 4675.
(18) Newstein, M. C.; Garetz, B. A.; Dai, H. J.; Balsara, N. P. *Macromolecules* **1995**, *28*, 4587.
(19) Dai, H. J.; Balsara, N. P.; Garetz, B. A.; Newstein, M. C. *Phys. Rev. Lett.* **1996**, *77*, 3677.
(20) Hashimoto, T.; Nakai, A.; Shiwaku, T.; Hasegawa, H.; Rojstaczer, S.; Stein, R. S. *Macromolecules* **1989**, *22*, 422.
(21) Rojstaczer, S. R.; Stein, R. S. *Macromolecules* **1990**, *23*, 4863.
(22) Perahia, D.; Vacca, G.; Patel, S. S.; Dai, H. J.; Balsara, N. P. *Macromolecules* **1994**, *27*, 7645.
(23) Flygare, W. H. *Molecular Structure and Dynamics*; Prentice-Hall: Englewood Cliffs, NJ, 1978.
(24) The parameters l and w in this paper are identical to those defined in ref 16 but are smaller than those in refs. 17 and 19 by a factor of $\sqrt{2}$. These differences arise from differences in the forms of the correlation functions used. The Gaussian parameters l and w in this paper can be related to equivalent ellipsoid shape function semimajor and semiminor axes a and b by the following relations: $l = (4/3)^{1/3}\pi^{1/12}a \approx 1.21a$ and $w = (4/3)^{1/3}\pi^{1/12}b$. We also point out a typographical error in eq 3 of ref 19: the hyperbolic Bessel function I_1 should be replaced by I_2.
(25) Netz, R. R.; Andelman, D.; Schick, M. *Phys. Rev. Lett.* **1997**, *79*, 1058.
(26) Carvalho, B. L.; Lescance, R. L.; Thomas, E. L *Macromol. Symp.* **1995**, *98*, 1131.
(27) Ohta, T.; Jasnow, D.; Kawasaki, K. *Phys. Rev. Lett.* **1982**, *49*, 1223.
(28) Balsara, N. P.; et al. Manuscript in preparation.
(29) Frost, H. J.; Thompson, C. V. *Curr. Opin. Solid State Mater. Sci.* **1996**, *1*, 361.

MA971086S